OUKA

The University of Osaka
Institutional Knowledge Archive

Title	Onset of intermittent thermal transport by ion-temperature-gradient-driven turbulence based on a low-degree-of-freedom model
Author(s)	Takeda, K.; Benkadda, S.; Hamaguchi, S. et al.
Citation	Physics of Plasmas. 2004, 11(7), p. 3561-3571
Version Type	VoR
URL	https://hdl.handle.net/11094/78487
rights	This article may be downloaded for personal use only. Any other use requires prior permission of the author and AIP Publishing. This article appeared in Physics of Plasmas 11, 3561 (2004) and may be found at https://doi.org/10.1063/1.1751175.
Note	

Onset of intermittent thermal transport by ion-temperature-gradient-driven turbulence based on a low-degree-of-freedom model

K. Takeda, S. Benkadda, S. Hamaguchi, and M. Wakatani

View Online

Export Citation

ARTICLES YOU MAY BE INTERESTED IN
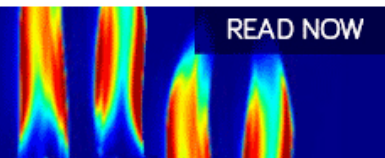
Onset of intermittent thermal transport by ion-temperature-gradient-driven turbulence based on a low-degree-of-freedom model

K. Takeda[a)]
Department of Fundamental Energy Science, Kyoto University, Gokasho, Uji, Kyoto 611-0011, Japan

S. Benkadda
Equipe Dynamique des Systèmes Complexes, Laboratoire PIIM, CNRS–Université de Provence, Marseille, France

S. Hamaguchi[b)] and M. Wakatani[c)]
Department of Fundamental Energy Science, Kyoto University, Gokasho, Uji, Kyoto 611-0011, Japan

Anomalous heat transport due to ion-temperature-gradient- (ITG)-driven turbulence is studied with the use of a low-degree-of-freedom model composed of 18 ordinary differential equations (ODEs). When the system is slightly above the stability threshold of ITG mode, the system is in the convection regime and convective heat transport of the system is time-independent or periodically oscillates. As the ion-temperature gradient is increased further, the system bifurcates to the turbulent regime. In the strongly turbulent regime, edge localized mode (ELM)-like intermittent bursts (so-called avalanches) are observed. This intermittency is caused by the competition of the following three factors: (1) generation of sheared flows and suppression of ITG turbulence, (2) gradual reduction of the sheared flows due to viscosity, and (3) rapid re-growth of ITG modes due to the reduction of the sheared flows. We found that the Nusselt number N_u scales with the ion pressure gradient K_i as $N_u \propto K_i^3$ in the presence of intermittent bursting transport. © *2004 American Institute of Physics.* [DOI: 10.1063/1.1751175]

I. INTRODUCTION

Turbulence driven by micro-instabilities in magnetically confined fusion experimental devices such as tokamaks have been extensively studied based on various simulation tools. One of the main goals of these studies is to clarify and control the anomalous transport and its relation with self-generated sheared flows, i.e., zonal flows. The presence of a self-generated sheared flow is known to be related with confinement improvement triggered by low to high confinement (L–H) transition in the edge region or the formation of an internal transport barrier (ITB) in the core region. Ion-temperature-gradient- (ITG)-driven turbulence is considered to be the major cause of anomalous ion thermal transport in the core region of a tokamak and many numerical simulations have demonstrated that self-generated sheared flows by ITG turbulence suppress the ITG turbulence and reduce the ion thermal transport across the magnetic surfaces.[1–4]

ITG modes have two branches, i.e., slab[5–8] and toroidal modes.[9–12] Either of these modes becomes unstable when the ratio of the normalized ion temperature gradient to normalized density gradient, η_i, becomes sufficiently large. The toroidal ITG mode is destabilized by η_i and ∇B-curvature drift, and this driving mechanism is similar to that of interchange instability. The toroidal ITG mode is localized in the outer region of the torus and generally has a higher growth

rate than the slab mode in toroidal magnetic geometry. In the present work, therefore, we focus on the toroidal ITG mode.

In order to understand nonlinear physics of interaction between convective transport and sheared plasma flows, low-degree-of-freedom dynamical models for the associated instability are sometimes more useful than its full fluid model. A low-degree-of-freedom model may be obtained from the projection of the dynamics governed by partial differential equations (PDEs) describing the instability to a small number of ordinary differential equations (ODEs). One of the most well-known and successful examples of such dynamical models is the Lorenz model for Rayleigh–Bénard convection.[13] Howard and Krishnamurti extended the Lorenz model to a 6 ODE system in order to include sheared flow formation in the problem of Rayleigh–Bénard convection.[14]

Dynamics of resistive interchange turbulence[15,16] was also studied based on similar ODE systems. Takayama *et al.* solved 5 and 7 ODE models for resistive interchange modes[17,18] and observed oscillations in kinetic energy and the Nusselt number. They also showed that sheared flows perpendicular to both the magnetic field and the direction of equilibrium pressure gradient are generated and suppress the resistive interchange turbulence. Bian *et al.*[19] presented another simple model for resistive interchange turbulence. The model contains only the fundamental mode in the poloidal direction but infinite degrees of freedom in the direction of pressure gradient (i.e., minor radius direction). With this mode, they have shown that intermittent bursts (so-called avalanches) takes place in the kinetic energy and convective

[a)]Electronic mail: takeda@center.iae.kyoto-u.ac.jp
[b)]Electronic mail: hamaguch@energy.kyoto-u.ac.jp
[c)]Deceased.

flux when the system is sufficiently unstable.

Unlike Rayleigh–Bénard convection or resistive interchange turbulence, drift wave modes such as ITG modes include wave solutions and intrinsically have twice as many degrees of freedom. For example, Hu and Horton[12] presented an 11 ODE model for toroidal ITG modes, with which they showed an L–H-like transition and oscillation in kinetic energy can take place. In the model, however, observed sheared flows were weak and no intermittent transport burst was observed. In this work, in order to clarify the role of sheared flows and transition dynamics for toroidal ITG modes, we have employed 18 degrees of freedom, instead of 11 that Hu and Horton used in Ref. 12, by including more radial mode numbers in the ODE model.

The rest of this article is organized as follows. In Sec. II, PDEs governing nonlinear ITG modes are presented and the projection of the system onto the 18 degrees of freedom space is given. We also present linear stability analysis and estimate the most unstable toroidal ITG mode under given conditions. In Sec. III, the numerical methods to solve the 18 ODE model are given. From the numerical solutions to these equations, we evaluate kinetic energy, Nusselt number, flux and Reynolds stress. These simulation results are given in Sec. IV. Discussion and summary are in Sec. V.

II. MODEL

A. Equations for toroidal ITG modes

Toroidal ITG modes may be given by the following vorticity and pressure equations:[9,12]

$$\frac{\partial}{\partial t}(\nabla_\perp^2\phi-\phi)+[\phi,\nabla_\perp^2\phi]=(1-g+K_i\nabla_\perp^2)\frac{\partial\phi}{\partial y}-g\frac{\partial p}{\partial y}$$

$$+\mu\nabla_\perp^2\nabla_\perp^2\phi, \tag{1}$$

$$\frac{\partial p}{\partial t}+[\phi,p]=-K_i\frac{\partial\phi}{\partial y}+\kappa\nabla_\perp^2 p, \tag{2}$$

where

$$[a,b]\equiv\frac{\partial a}{\partial x}\frac{\partial b}{\partial y}-\frac{\partial a}{\partial y}\frac{\partial b}{\partial x}, \tag{3}$$

is the Poisson bracket. Modes we consider in this work are two dimensional (2D) and the magnetic shear is neglected. The normalized variables x and y indicate coordinates in the radial and poloidal directions and the constant magnetic field is assumed to be in the z direction. In the equations above, $g=2L_n/R$ is the effective gravity due to the curvature of magnetic field, $K_i=T_i/T_e(\eta_i+1)$ with T_i and T_e being the ion and electron temperatures is a parameter proportional to the equilibrium ion pressure gradient, where $\eta_i=d\ln T_i/d\ln n$, n is the plasma density, μ is the viscosity, and κ is the thermal conductivity. In Eqs. (1) and (2), the standard drift wave units $x\equiv x/\rho_s$, $y\equiv y/\rho_s$, $t\equiv(L_n/c_s)t$, $p\equiv L_nT_{i0}/(\rho_s P_{i0}T_{e0})p$, $\phi\equiv eL_n/(B_0T_{e0}\rho_s)\phi$, $\mu\equiv eL_n/(B_0T_{e0}\rho_s)\mu$, and $\kappa\equiv eL_n/(B_0T_{e0}\rho_s)\kappa$ are used, where c_s is the ion sound velocity, $\rho_s=c_s/\Omega_i$, Ω_i is the ion cyclotron frequency, and subscript 0 indicates the equilibrium quantities.

In numerical calculations presented in this article, we used $g=0.05$, $\mu=0.04$, and $\kappa=0.01$. Equations (1) and (2) are solved in a rectangular region $0\leq x\leq L_x$ and $0\leq y\leq L_y$ with perfectly conducting walls being located at $x=0$ and $x=L_x$. Periodic boundary conditions are imposed in the y direction and $\phi(x=0,L_x)=0$ and $p(x=0,L_x)=0$ are assumed at the wall. The normalized equilibrium ion pressure (temperature) gradient K_i (η_i) is a parameter of Eqs. (1) and (2) that controls the growth rate of ITG mode.

B. Linear analysis

We now carry out linear analysis of Eqs. (1) and (2) to obtain the most unstable mode. Assuming a fluctuation of the form $\exp(k_x x+k_y y-i\omega t)$ with $k_x=\pi/L_x$ and $k_y=2\pi/L_y$ and linearizing Eqs. (1) and (2), we obtain the dispersion relation as follows:

$$[-i(1+k_\perp^2)\omega+ik_y(1-g-K_ik_\perp^2)+\mu k_\perp^2](-i\omega+\kappa k_\perp^2)$$

$$-gK_ik_y^2=0. \tag{4}$$

This is a quadratic equation which can be solved with respect to ω as

$$\omega=\frac{1}{2(1+k_\perp^2)}\{k_y(1-g-K_ik_\perp^2)-i[\kappa k_\perp^2(1+k_\perp^2)$$

$$+\mu k_\perp^4]\pm\sqrt{D_k}\}, \tag{5}$$

where

$$D_k=\{k_y(1-g-K_ik_\perp^2)+i[\kappa k_\perp^2(1+k_\perp^2)-\mu k_\perp^4]\}^2$$

$$-4(1+k_\perp^2)gK_ik_y^2. \tag{6}$$

The linear growth rate is derived from $\gamma=\text{Im}(\omega)$. It follows that the system becomes unstable if

$$\frac{(1-g-K_ik_\perp^2)^2k_\perp^2k_y^2\mu/\kappa}{[1+k_\perp^2(1+\mu/\kappa)]^2}+\mu\kappa k_\perp^6-gK_ik_y^2<0 \tag{7}$$

is satisfied. It is clear from this condition that the most unstable mode has the wave numbers satisfying

$$k_x^2\ll k_y^2\sim k_\perp^2=\frac{1-g}{K_i}. \tag{8}$$

In this paper, we assume $k_x=k_y/2$ for the sake of simplicity, and set

$$k_x=k_y/2=[(1-g)/5K_i]^{1/2}, \tag{9}$$

so that this mode satisfies Eq. (8).

C. The low-degree-of-freedom model of 18 ODEs

Using the most unstable mode selected in the previous subsection and a small number of higher harmonics, i.e., $(\ell k_x,mk_y)$ with $1\leq\ell\leq3$ and $0\leq m\leq1$, we reduced the PDEs (1) and (2) to the set of ODEs. The selected components for ϕ and p are given by the following expressions:

$$\phi(x,y,t) = \phi_1^0(t)\sin(k_x x) + \phi_2^0(t)\sin(2k_x x) + \phi_3^0(t)\sin(3k_x x) + \phi_1^c(t)\sin(k_x x)\cos(k_y y) + \phi_1^s(t)\sin(k_x x)\sin(k_y y)$$
$$+ \phi_2^c(t)\sin(2k_x x)\cos(k_y y) + \phi_2^s(t)\sin(2k_x x)\sin(k_y y) + \phi_3^c(t)\sin(3k_x x)\cos(k_y y) + \phi_3^s(t)\sin(3k_x x)\sin(k_y y),$$

$$(10)$$

$$p(x,y,t) = p_1^0(t)\sin(k_x x) + p_2^0(t)\sin(2k_x x) + p_3^0(t)\sin(3k_x x) + p_1^c(t)\sin(k_x x)\cos(k_y y) + p_1^s(t)\sin(k_x x)\sin(k_y y)$$
$$+ p_2^c(t)\sin(2k_x x)\cos(k_y y) + p_2^s(t)\sin(2k_x x)\sin(k_y y) + p_3^c(t)\sin(3k_x x)\cos(k_y y) + p_3^s(t)\sin(3k_x x)\sin(k_y y).$$

$$(11)$$

This is an extension of the Hu–Horton model,[12] which include 11 components, i.e., $(\ell k_x, m k_y)$ modes with $1 \le \ell \le 2$ and $0 \le m \le 1$. The only difference between our model and the Hu–Horton model is the presence of $(3k_x, k_y)$ mode in our model.[20] Note that sheared flow components, i.e., $\phi_1^0(t)$, $\phi_2^0(t)$, and $\phi_3^0(t)$, are also included.

Substituting these equations to Eqs. (1) and (2), we obtain the 18 coupled ordinary differential equations for each harmonics. The complete set of ODEs are given in the Appendix.

III. DEFINITIONS OF QUANTITIES CHARACTERIZING THE SYSTEM

The 18 ODEs (A1)–(A18) given in the Appendix are solved numerically with fifth-order Runge–Kutta method. In this section, we define characteristic quantities of the system that can be evaluated from the numerical solutions. The kinetic energy of the system may be defined as

$$K = \int \phi^2 + (\nabla_\perp \phi)^2 dV/V = \langle \phi^2 + (\nabla_\perp \phi)^2 \rangle_V, \qquad (12)$$

where V denotes the total volume of the system and $\langle \rangle_V$ means the volume average. The kinetic energies for the mean shear flow (i.e., the $m=0$ mode) and for different radial components for the fundamental mode (i.e., the $m=1$ mode) may be defined as

$$K_0 = \sum_{\ell=1}^{3} \frac{1}{4}(1 + \ell^2 k_x^2)(\phi_\ell^0)^2, \qquad (13)$$

$$K_\ell = \frac{1}{8}(1 + \ell^2 k_x^2 + k_y^2)[(\phi_\ell^c)^2 + (\phi_\ell^s)^2] \quad (\ell=1,2,3). \qquad (14)$$

It should be noted that the plasma mean flow in the y direction, i.e., $V_y(x,t) = -\langle \partial\phi/\partial x \rangle_y$ with $\langle \rangle_y = \int dy/L_y$, is characterized by the $m=0$ mode of electric potential ϕ, i.e., $\langle \phi \rangle_y = \phi_1^0(t)\sin(k_x x) + \phi_2^0(t)\sin(2k_x x) + \phi_3^0(t)\sin(3k_x x)$.

Sheared flows are generated by turbulence via Reynolds stress, which may be defined as a function of the radial position x as

$$S_R(x,t) = \langle v_x v_y \rangle_y, \qquad (15)$$

with $v_x = \partial\phi/\partial y$ and $v_y = -\partial\phi/\partial x$.

The quantities characterizing anomalous heat transport of the system, i.e., convective thermal flux and Nusselt number may be defined as

$$\Gamma(x,t) = \int p v_x dy/L_y = \langle p v_x \rangle_y \qquad (16)$$

and

$$N_u(t) = \int \kappa K_i + p v_x \frac{dV}{V} \Big/ (\kappa K_i) = 1 + \frac{\langle p v_x \rangle_V}{\kappa K_i}. \qquad (17)$$

Note that the Nusselt number is the ratio of the total heat flux (i.e., the sum of the convective and conductive fluxes) to the conductive heat flux. The Nusselt number is typically high when the system is in turbulent state, where the convective flux is usually much higher than the conductive flux.

IV. SIMULATION RESULTS

When $K_i = 0.3$, i.e., the control parameter K_i is slightly above the stability threshold K_{ic} (under the parameters we employed in this work, $K_{ic} \simeq 0.21$), the system reaches another steady state with finite convective flows. Figure 1 shows the time evolution of the kinetic energies and Nusselt number. The trajectory in the phase space "sheared flows energy K_0–Nusselt number N_u" is shown in Fig. 2(a), which indicates that the system converges to a fixed steady state. The power spectrum of the kinetic energy of the 1st harmonics K_1 is given in Fig. 2(b), where the spectrum is peaked only at zero frequency, i.e., $f=0$.

Time evolutions of the kinetic energies and Nusselt number in the case of $K_i = 0.4$ are shown in Fig. 3. Periodic
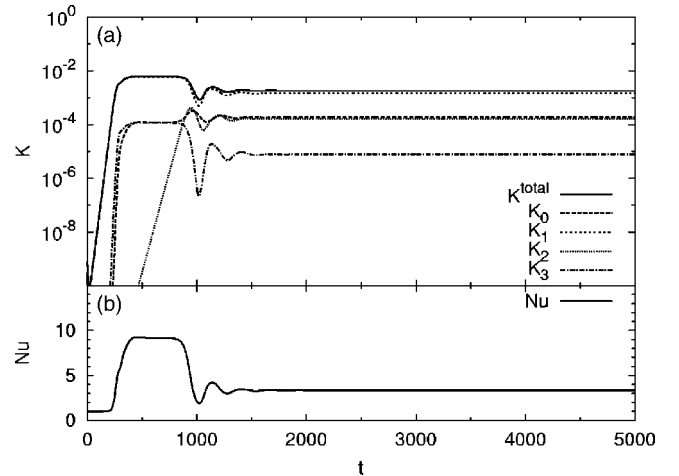

FIG. 1. Time evolutions of kinetic energy (a) and N_u (b) in the case of $K_i = 0.3$. In (a), K_1 is dominant and nearly equal to K. In the steady state, $K_0 \simeq K_2$, which are about one tenth of K_1.
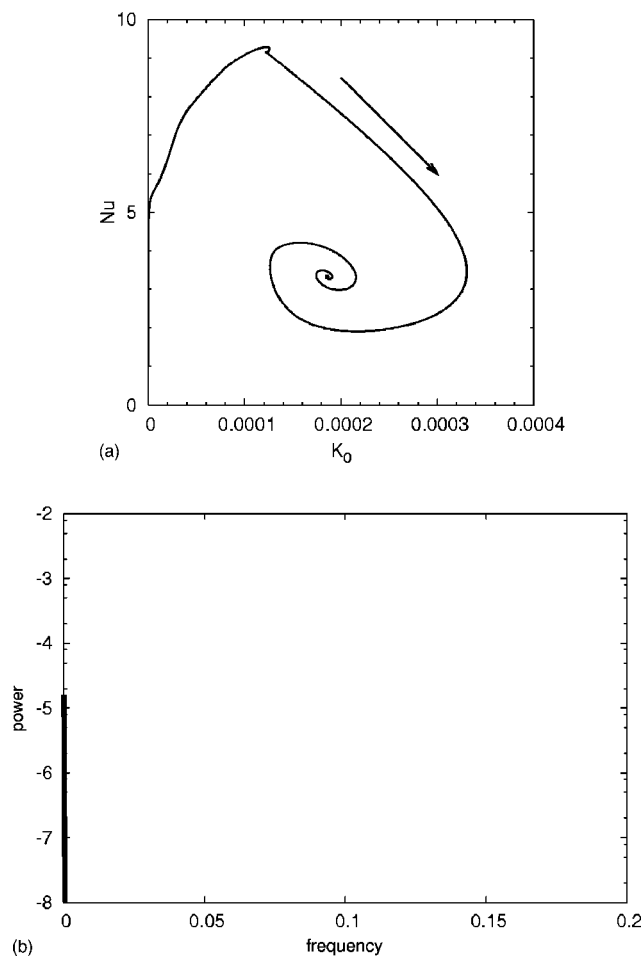
(a)

(b)

FIG. 2. Phase space "K_0-N_u" (a) and power spectrum of K_1 (b) in the case of $K_i=0.3$. In (b), the peak is located on at zero frequency, i.e., $f=0$.

(a)

(b)

FIG. 4. Phase space "K_0-N_u" (a) and power spectrum of K_1 (b) in the case of $K_i=0.4$.

oscillations in these quantities are observed. Figure 4 shows (a) the trajectory in the "K_0-N_u" phase space and (b) the power spectrum of K_1. Time evolution is governed by a single frequency mode and the trajectory in the phase space is attracted to a simple limit cycle.
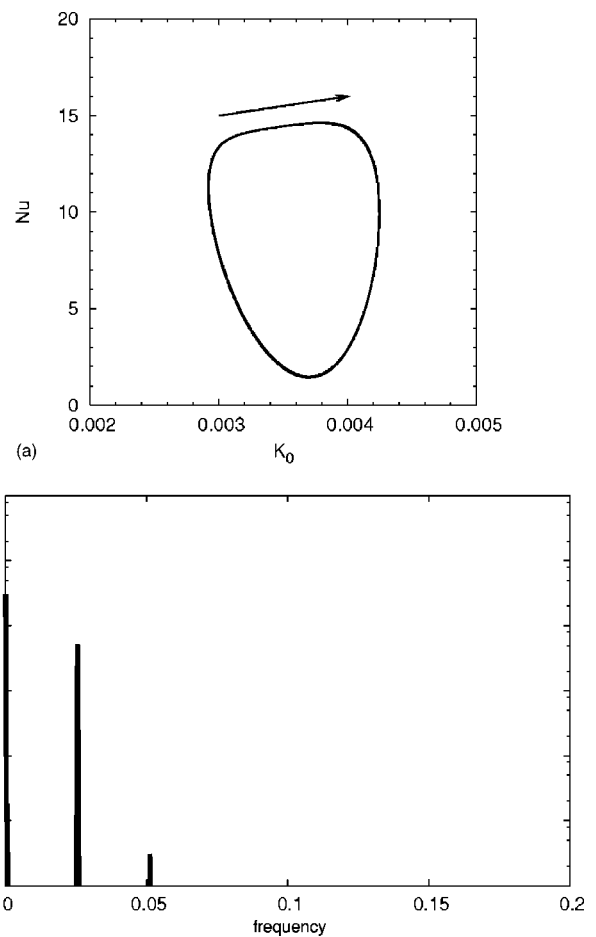
Figure 5 shows time evolutions of the kinetic energies and Nusselt number, and Fig. 6 shows the trajectory in the "K_0-N_u" phase space and (b) power spectrum of K_1. The frequencies of oscillations change as K_i increases but the system still exhibits periodic oscillations. Figure 6(a) shows that the trajectory in the phase space converges to a different
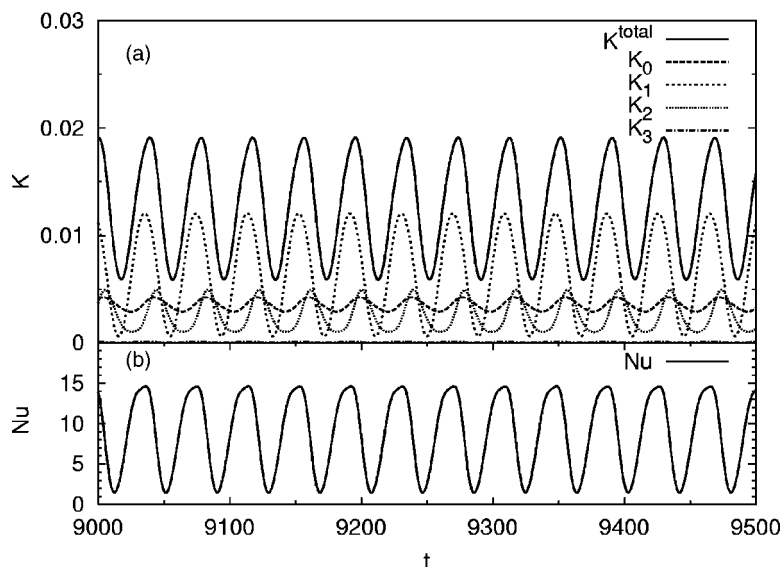

FIG. 3. Time evolutions of kinetic energy (a) and N_u (b) in the case of $K_i=0.4$. In (a) K_1 is dominant and K_3 is too small to be seen.
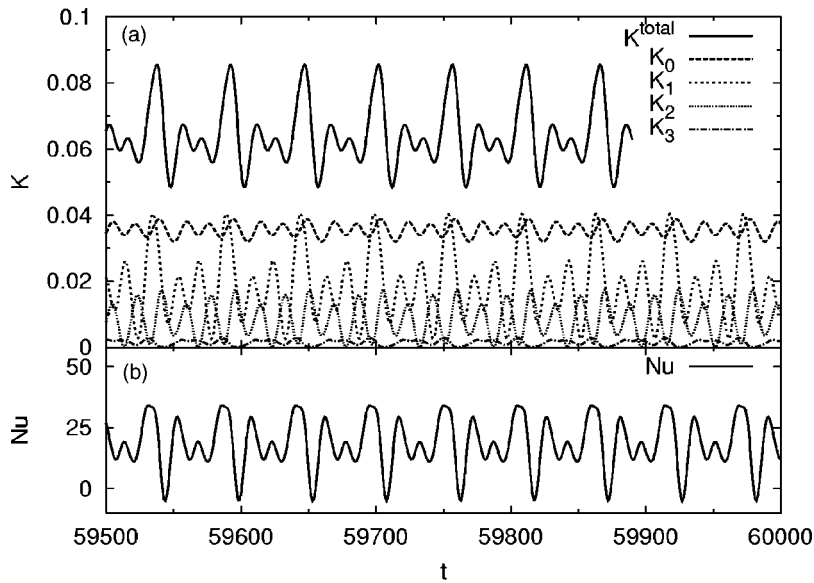
FIG. 5. Time evolutions of kinetic energy (a) and N_u (b) in the case of $K_i = 0.5$.

type of limit cycle. More higher harmonics in the oscillation frequencies are seen in Fig. 6(b).

When K_i is slightly more increased and set to be 0.6, the system bifurcates to a chaotic state as shown in Figs. 7 and 8. Time evolutions of the kinetic energy and Nusselt number are no longer periodic oscillations. The system exhibits a complex trajectory in the phase space "$K_0 - N_u$" as shown in Fig. 8(a). Figure 8(b) shows that K_1 has a continuous spectrum, which indicates that the system is indeed in a chaotic state.

If K_i is further increased and set to be $K_i \gtrsim 3$, the system becomes strongly turbulent. Under such conditions, fluctuations exhibit intermittent bursts.

In the case of $K_i = 4.0$, time evolution of the kinetic energies, Nusselt number, and Reynolds stress (averaged over x) are shown in Figs. 9 and 10. In these figures, intermittent explosive rises of these quantities are clearly seen. Such time evolution of the physical quantities may be explained by the following mechanism. When the ITG modes grow and turbulence is developed, sheared flows are generated through the Reynolds stress as shown in Fig. 10(b). In this phase, fluctuations are burst-like and their levels are high. We call this phase the "bursting phase." Increased sheared flows then suppress the ITG modes, terminating the source of sheared flows in the system. The sheared flows generated earlier by the ITG modes continue to exist for a while but gradually decay due to viscous damping. In this phase, both sheared flows (which can be measured by K_0) and convective heat transport (which can be measured by N_u) gradually decay and the flow structures are more or less laminar, as we shall see in Fig. 12 below. We call this phase the "laminar phase." As the sheared flows continue to decay, the ITG modes begin to grow again. As convective cells due to ITG instabilities tend to tilt in this phase, we call this phase the "tilting phase." Eventually the magnitudes of sheared flows becomes sufficiently low and the system returns to the "bursting phase." As we can readily see in Figs. 9 and 10, the Nusselt number and Reynolds stress burst when ITG modes grow rapidly. For realistic deuterium plasmas with $T_e \sim 2$ keV and $L_n \sim 30$ cm, the time period of intermittency obtained here corresponds to about 10 ms.

The trajectories in the phase space "$K_0 - N_u$" are given in Fig. 11 for the (a) bursting, (b) laminar, and (c) tilting
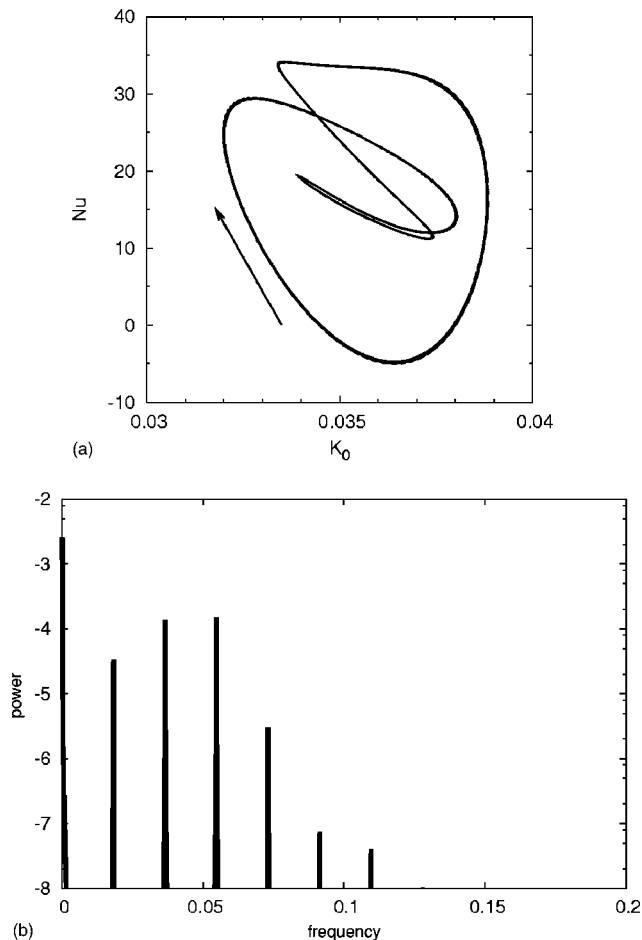

FIG. 6. Phase space "$K_0 - N_u$" (a) and power spectrum of K_1 (b) in the case of $K_i = 0.5$.
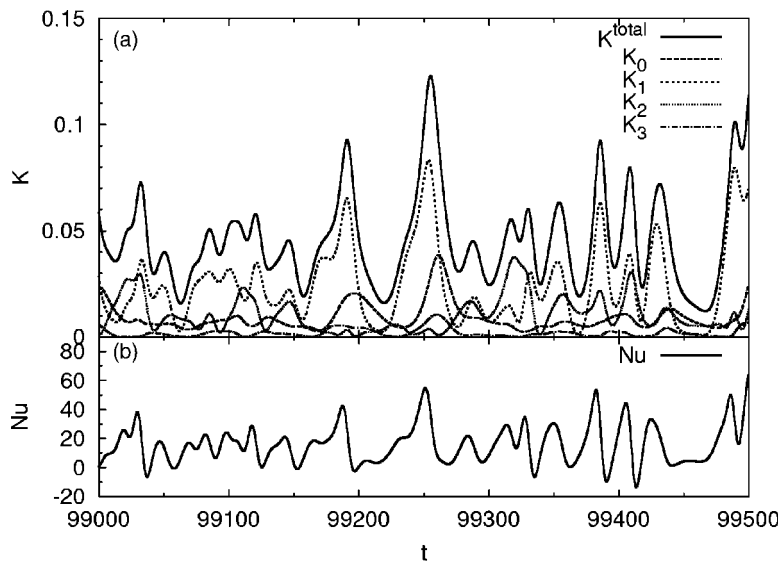
FIG. 7. Time evolutions of kinetic energy (a) and N_u (b) in the case of $K_i=0.6$.

phases. In the bursting phase the system is in a strongly turbulent state and the trajectory is far more complex than those in any other phases. We also note that the magnitudes of K_0 and Nu can be vary large. In the laminar phase the system follows a regular trajectory with both the value of K_0

FIG. 8. Phase space "K_0-N_u" (a) and power spectrum of K_1 (b) in the case of $K_i=0.6$.

and the oscillation amplitude of Nu decreasing gradually. The decrease of K_0, i.e., the energy of sheared flows, is due to viscous damping. In the tilting phase the sheared flows continue to decrease, but Nu, i.e., the convective heat transport, gradually increase due to the re-excitation of ITG instabilities.

Contours of the electrostatic potential function $\phi(x,y,t)$ in real space are presented in Fig. 12 for the same simulation run. Typical potential contours in the bursting phase are given in Fig. 12(a), those in the laminar phase are given in Figs. 12(b) and 12(c), and those in the tilting phase are given in Figs. 12(d) and 12(e). In Fig. 12(a), ITG turbulence governs the system and typical ITG nonlinear mode structures appear in the potential contours. In Fig. 12(b), sheared flows are dominant and ITG modes are sufficiently suppressed. After sheared flows become weak due to viscous damping, convection cells arising from ITG instabilities grow and often tilt, as shown in Fig. 12(c).

Space–time contour of the poloidally (i.e., y-) averaged electrostatic potential $\langle\phi\rangle_y(x,t)$ is shown in Fig. 13 for the simulation run given in Fig. 9. It is readily seen that ϕ_1^0 is the dominant component after each bursts. It should be noted that all three modes considered here, i.e., ϕ_1^0, ϕ_2^0 and ϕ_3^0, equally contribute to the generation of sheared flows. However we observe that ϕ_2^0 and ϕ_3^0 decay much faster than ϕ_1^0 due to viscous damping. Therefore the period of intermittency is essentially determined by the decay rate of ϕ_1^0, i.e., the $\ell=1$ component of sheared flow.

Dependence of the time averaged Nusselt number N_u on the parameter K_i is described in Fig. 14. The time average of instantaneous $N_u(t)$ is taken over a sufficiently long period and the errors arising from the time average process are confirmed to be negligibly small in this figure. The scaling $N_u \propto K_i^3$ is readily seen in this figure when $K_i \gtrsim 4$ and $K_i \lesssim 0.9$. The proportional coefficients in $K_i \gtrsim 4$ and $K_i \lesssim 0.9$ are clearly different. When $K_i \gtrsim 3$, where intermittent bursts of heat transport and other fluctuating quantities are observed, the magnitude of Nu is lower than the value of straightforward extension of the Nu scaling observed in the region of
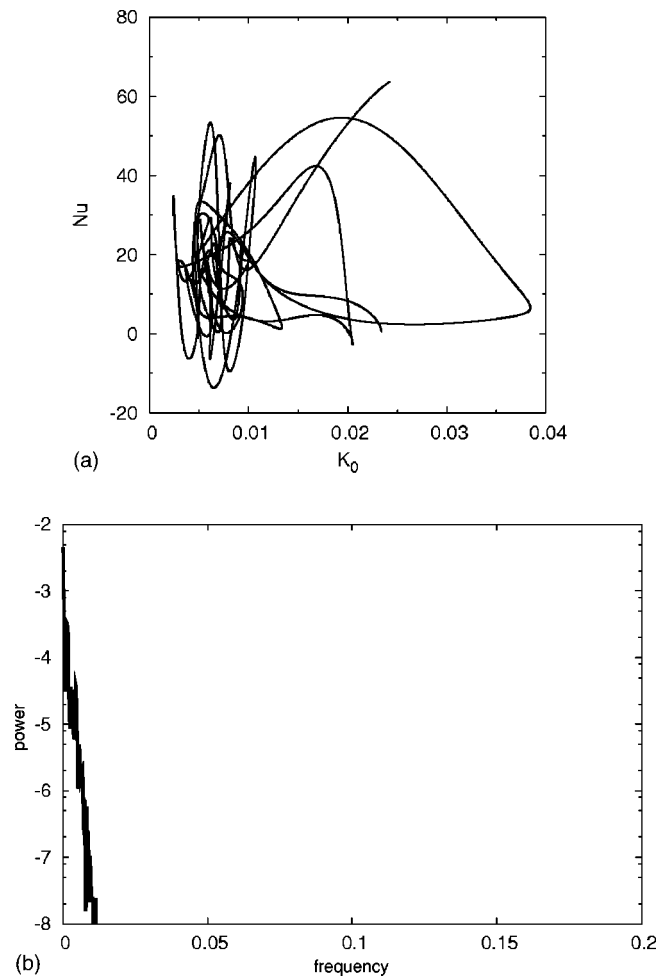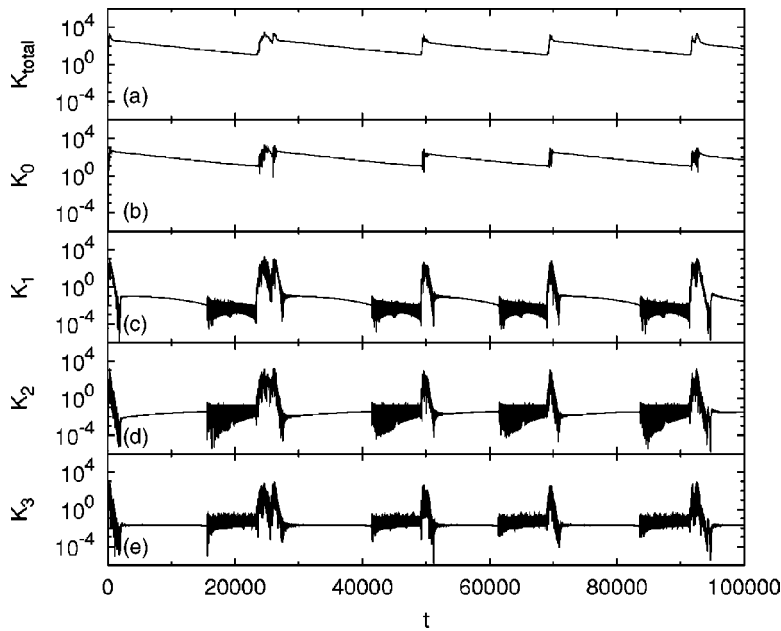
FIG. 9. Time evolution of total kinetic energy K (a), and kinetic energies of sheared flows K_0 (b), the 1st harmonics K_1 (c), the 2nd harmonics K_2 (d), and the 3rd harmonics K_3 (e) in the case of $K_i = 4$.

$K_i \lesssim 0.9$. Suppression of ITG modes by the self-generated sheared flows significantly reduces convective heat transport for extended periods during the discharge, which clearly contributes to the reduction of the proportional coefficient of the scaling law given above.

V. DISCUSSION

We have examined nonlinear evolution of convective heat transport and other physical quantities of plasmas which are subject to ITG instabilities, using a low-degree-of-freedom model composed of 18 ODEs. When the system is slightly above the ITG stability threshold, i.e., the control parameter $K_i \gtrsim K_{ic}$, ITG driven convections reach a steady state. As we increase K_i slightly more, periodic oscillations in the kinetic energy and convective heat transport (i.e., N_u)

are observed. If K_i is further increased, the system bifurcates to a turbulent regime. When the turbulence is sufficiently strong, ELM-like intermittent bursts, so called avalanches, are observed. This contrasts with the simulation results based on the 11 ODE model studied by Hu and Horton,[12] where no intermittent bursts were reported. We have found that the intermittency we observed in our 18 ODE model is caused by the competition of the following 3 factors; (1) generation of sheared flows and suppression of ITG turbulence, (2) gradual reduction of the sheared flows due to viscosity, and (3) rapid re-growth of ITG modes due to the reduction of the sheared flows. We found that the Nusselt number N_u scales with the ion pressure gradient K_i as $N_u \propto K_i^3$ in the presence of intermittent bursting transport.

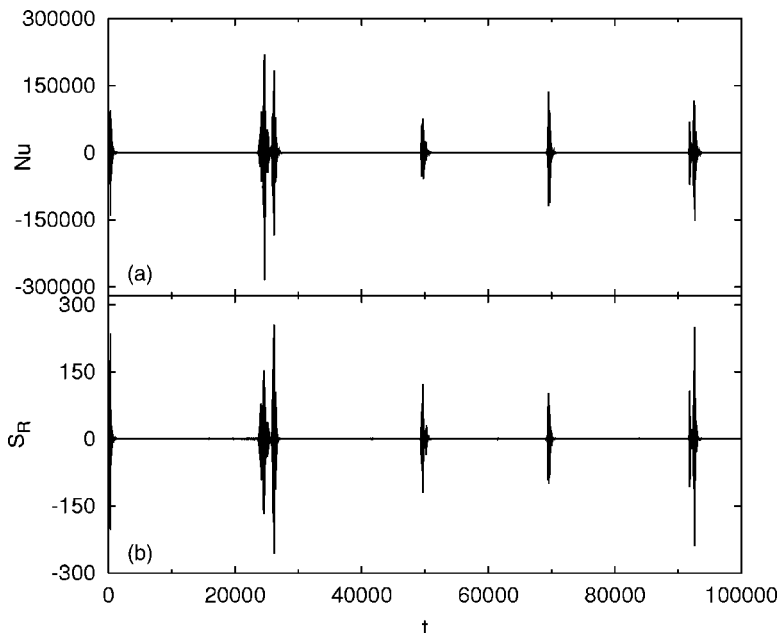It should be noted that the role of viscosity is essential

FIG. 10. Time evolutions of the Nusselt number N_u (a) and the Reynolds stress S_R (b) in the case of $K_i = 4$.
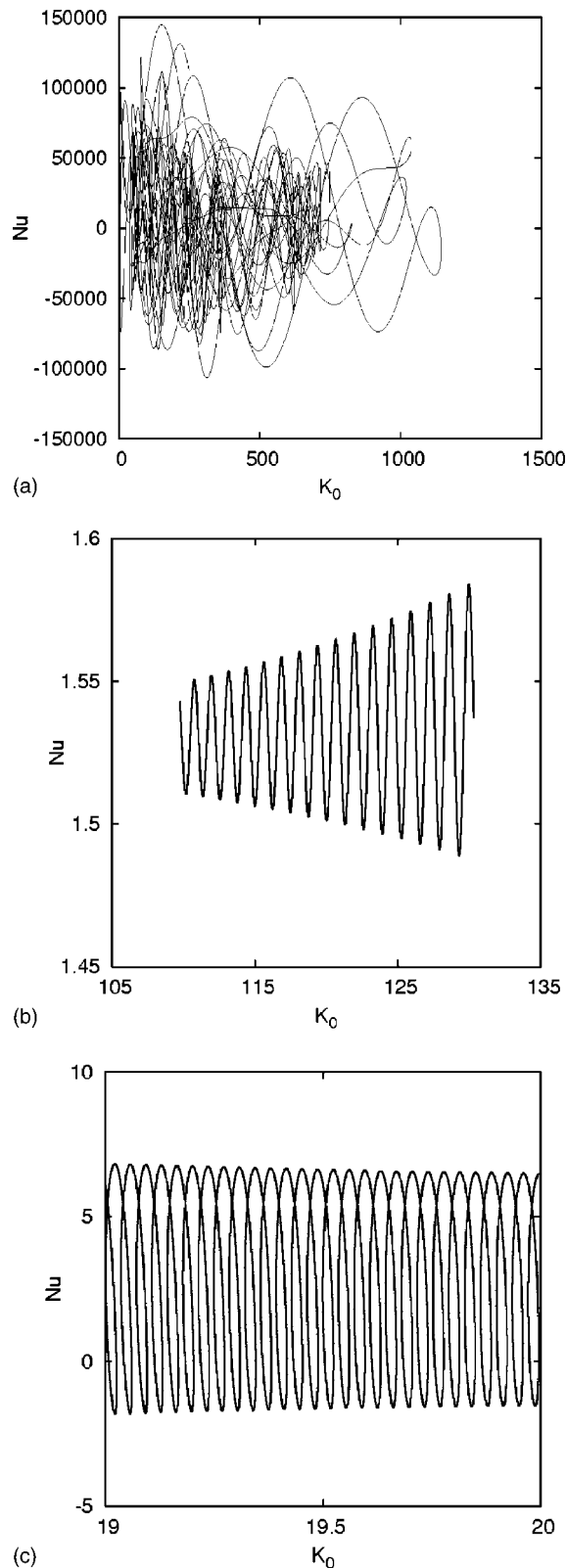
(a)

(b)

(c)

FIG. 11. Phase space "$K_0 - N_u$" in the bursting phase (a), the laminar phase (b), and the tilting phase (c) in the case of $K_i = 4$.

mittent oscillation of zonal flows generated by ITG turbulence has been observed in gyro-kinetic simulations by Lin et al.[21]

We have confirmed by dropping higher order harmonics in Eqs. (10) and (11) that the 11 ODE model does not exhibit such intermittency and instead shows random oscillations of kinetic energies K_n when the system is strongly unstable. In a 16 ODE model in which only ϕ_2^0 and ϕ_3^0 are neglected, the intermittency was recovered and ϕ_1^0 is observed to be dominant in the laminar phase. Indeed, under the 18 ODE model, ϕ_2^0 and ϕ_3^0 are generated through nonlinear mode coupling of ITG modes but dissipate rapidly by viscosity. It follows that, for intermittency to occur, velocity shear generated by ϕ_1^0 plays the essential role to suppress the ITG mode. We have also observed that the time period of intermittency is essentially determined by the decay rate of the ϕ_1^0 component of sheared flow energy.

In the case of resistive interchange turbulence, oscillatory behavior is also observed by using the 5–7 ODE models[17,18,22] but no intermittent bursts were reported to be observed under these models. On the other hand, using a simple nonlinear model of resistive interchange modes that retains only the fundamental mode in the poloidal direction and infinite degrees of freedom in the radial direction (i.e., the full x dependence of all dependent variables, which are discretized by means of a finite differential method), Bian et al.[19] demonstrated that intermittent bursts of convective heat transport occurs. It follows that, for resistive interchange modes, one needs at least some higher harmonics in the x direction in order to reproduce intermittent burst-like convective heat transport.

The toroidal ITG mode is a drift wave instability and therefore requires twice the number of degrees of freedom compared with the resistive interchange mode but the driving mechanisms of these instabilities are similar. In this sense it is worth comparing our simulation results of ITG turbulence with those of resistive interchange turbulence mentioned above. The simulation results for Hu and Horton's 11 ODE model for ITG modes suggests that this model corresponds to the 5, 6, or 7 ODE model for resistive interchange modes in the sense that neither of them contains sufficiently high harmonics in the x direction to reproduce intermittent burst-like heat transport. Therefore, one may consider that the 18 ODE model for ITG modes that we employed in this work corresponds to an intermediate degree-of-freedom model between the 5, 6, or 7 ODE model and Bian's model with infinite degrees of freedom in the x direction. Our simulation results indicate that at least third harmonics in the x direction must be included in order to obtain intermittent oscillations.

ACKNOWLEDGMENTS

for the occurrence of intermittency. We have indeed confirmed that, without viscosity, i.e., $\mu = 0$, no intermittency was observed. With finite viscosity, the system is said to be in a state of self-organized criticality (SOC). Similar inter-
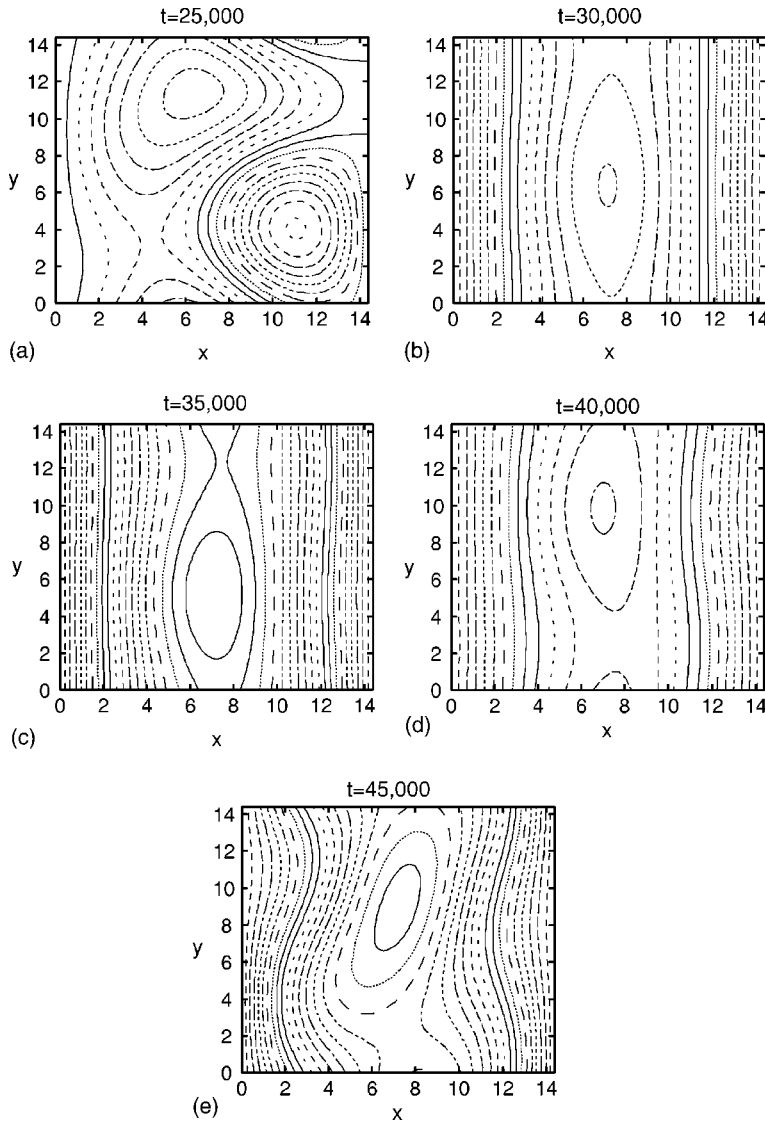
FIG. 12. Real space contour of $\phi(x,y,t)$ in the bursting phase [at $t=25\,000$ (a)], the laminar phase [at $t=30\,000$ (b) and $t=35\,000$ (c)], and the tilting phase [at $t=40\,000$ (d) and $t=45\,000$ (e)].

APPENDIX: 18 MODE COUPLING EQUATIONS

Here we present the low-degree-of-freedom model used in this work. Substituting the Eqs. (10) and (11) to the Eqs. (1) and (2), we obtain the following 18 coupled ODEs:

$$(1+k_x^2)\frac{d\phi_1^0}{dt} = \frac{k_{xy}^2}{2}k_x^2\{3(\phi_1^c\phi_2^s - \phi_1^s\phi_2^c)$$
$$+5(\phi_2^c\phi_3^s - \phi_2^s\phi_3^c)\} - \mu k_x^4\phi_1^0, \qquad (A1)$$

$$(1+4k_x^2)\frac{d\phi_2^0}{dt} = 8k_{xy}^2k_x^2(\phi_1^c\phi_3^s - \phi_1^s\phi_3^c) - 16\mu k_x^4\phi_2^0, \qquad (A2)$$

$$(1+9k_x^2)\frac{d\phi_3^0}{dt} = \frac{9}{2}k_{xy}^2k_x^2(\phi_1^s\phi_2^c - \phi_1^c\phi_2^s) - 81\mu k_x^4\phi_3^0, \qquad (A3)$$
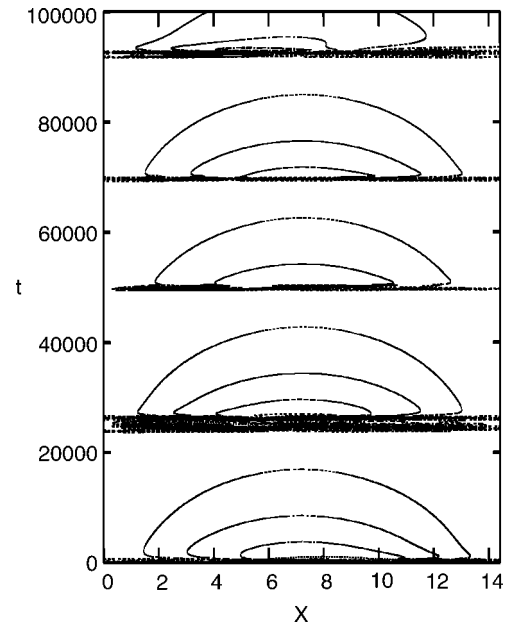

FIG. 13. Space–time contours of the y averaged electrostatic potential $\langle\phi\rangle_y(x,t)$ in the case of $K_i=4$.
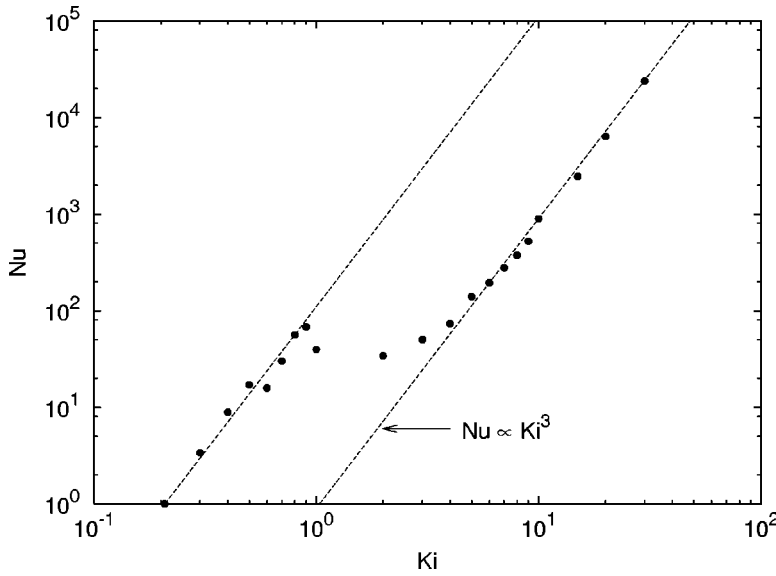
FIG. 14. Time averaged Nusselt number N_u as a function of K_i. Broken lines represent $N_u \propto K_i^3$.

$$(1+k_1^2)\frac{d\phi_1^c}{dt} = -k_{xy}^2\{(k_2^2-k_x^2)\phi_1^0\phi_2^s - 2(k_1^2-4k_x^2)\phi_2^0\phi_1^s$$
$$+ 2(k_3^2-4k_x^2)\phi_2^0\phi_3^s - 3(k_2^2-9k_x^2)\phi_3^0\phi_2^s\}$$
$$-(1-g-K_ik_1^2)k_y\phi_1^s + gk_yp_1^s - \mu k_1^4\phi_1^c, \tag{A4}$$

$$(1+k_1^2)\frac{d\phi_1^s}{dt} = k_{xy}^2\{(k_2^2-k_x^2)\phi_1^0\phi_2^c - 2(k_1^2-4k_x^2)\phi_2^0\phi_1^c$$
$$+ 2(k_3^2-4k_x^2)\phi_2^0\phi_3^c - 3(k_2^2-9k_x^2)\phi_3^0\phi_2^c\}$$
$$+(1-g-K_ik_1^2)k_y\phi_1^c - gk_yp_1^c - \mu k_1^4\phi_1^s, \tag{A5}$$

$$(1+k_2^2)\frac{d\phi_2^c}{dt} = -k_{xy}^2\{(k_1^2-k_x^2)\phi_1^0\phi_1^s + (k_3^2-k_x^2)\phi_1^0\phi_3^s$$
$$- 3(k_1^2-9k_x^2)\phi_3^0\phi_1^s\} - (1-g$$
$$- K_ik_2^2)k_y\phi_2^s + gk_yp_2^s - \mu k_2^4\phi_2^c, \tag{A6}$$

$$(1+k_2^2)\frac{d\phi_2^s}{dt} = k_{xy}^2\{(k_1^2-k_x^2)\phi_1^0\phi_1^c + (k_3^2-k_x^2)\phi_1^0\phi_3^c$$
$$- 3(k_1^2-9k_x^2)\phi_3^0\phi_1^c\} + (1-g$$
$$- K_ik_2^2)k_y\phi_2^c - gk_yp_2^c - \mu k_2^4\phi_2^s, \tag{A7}$$

$$(1+k_3^2)\frac{d\phi_3^c}{dt} = -k_{xy}^2\{(k_2^2-k_x^2)\phi_1^0\phi_2^s + 2(k_1^2$$
$$- 4k_x^2)\phi_2^0\phi_1^s\} - (1-g-K_ik_3^2)k_y\phi_3^s$$
$$+ gk_yp_3^s - \mu k_3^4\phi_3^c, \tag{A8}$$

$$(1+k_3^2)\frac{d\phi_3^s}{dt} = k_{xy}^2\{(k_2^2-k_x^2)\phi_1^0\phi_2^c + 2(k_1^2-4k_x^2)\phi_2^0\phi_1^c\}$$
$$+(1-g-K_ik_3^2)k_y\phi_3^c - gk_yp_3^c - \mu k_3^4\phi_3^s, \tag{A9}$$

$$\frac{dp_1^0}{dt} = \frac{k_{xy}^2}{2}\{p_1^s\phi_2^c - p_1^c\phi_2^s + p_2^s\phi_1^c - p_2^c\phi_1^s + p_3^s\phi_2^c - p_3^c\phi_2^s$$
$$+ p_2^s\phi_3^c - p_2^c\phi_3^s\} - \kappa k_x^2 p_1^0, \tag{A10}$$

$$\frac{dp_2^0}{dt} = k_{xy}^2\{p_1^c\phi_1^s - p_1^s\phi_1^c + p_1^c\phi_3^s - p_1^s\phi_3^c + p_3^c\phi_1^s - p_3^s\phi_1^c\}$$
$$- 4\kappa k_x^2 p_2^0, \tag{A11}$$

$$\frac{dp_3^0}{dt} = -\frac{3k_{xy}^2}{2}\{p_1^s\phi_2^c - p_1^c\phi_2^s + p_2^s\phi_1^c - p_2^c\phi_1^s\} - 9\kappa k_x^2 p_3^0, \tag{A12}$$

$$\frac{dp_1^c}{dt} = k_{xy}^2\{(p_1^0\phi_2^s - p_2^s\phi_1^0) - 2(p_2^0\phi_1^s - p_1^s\phi_2^0) + 2(p_2^0\phi_3^s$$
$$- p_3^s\phi_2^0) - 3(p_3^0\phi_2^s - p_2^s\phi_3^0)\} - K_ik_y\phi_1^s - \kappa k_1^2 p_1^c, \tag{A13}$$

$$\frac{dp_1^s}{dt} = -k_{xy}^2\{(p_1^0\phi_2^c - p_2^c\phi_1^0) - 2(p_2^0\phi_1^c - p_1^c\phi_2^0) + 2(p_2^0\phi_3^c$$
$$- p_3^c\phi_2^0) - 3(p_3^0\phi_2^c - p_2^c\phi_3^0)\} + K_ik_y\phi_1^c - \kappa k_1^2 p_1^s, \tag{A14}$$

$$\frac{dp_2^c}{dt} = k_{xy}^2\{(p_1^0\phi_1^s - p_1^s\phi_1^0) + (p_1^0\phi_3^s - p_3^s\phi_1^0)$$
$$- 3(p_3^0\phi_1^s - p_1^s\phi_3^0)\} - K_ik_y\phi_2^s - \kappa k_2^2 p_2^c, \tag{A15}$$

$$\frac{dp_2^s}{dt} = -k_{xy}^2\{(p_1^0\phi_1^c - p_1^c\phi_1^0) + (p_1^0\phi_3^c - p_3^c\phi_1^0)$$
$$- 3(p_3^0\phi_1^c - p_1^c\phi_3^0)\} + K_ik_y\phi_2^c - \kappa k_2^2 p_2^s, \tag{A16}$$

$$\frac{dp_3^c}{dt} = k_{xy}^2\{(p_1^0\phi_2^s - p_2^s\phi_1^0) + 2(p_2^0\phi_1^s - p_1^s\phi_2^0)\} - K_ik_y\phi_3^s$$
$$- \kappa k_3^2 p_3^c, \tag{A17}$$

$$\frac{dp_3^s}{dt} = -k_{xy}^2 \{(p_1^0 \phi_2^c - p_2^c \phi_1^0) + 2(p_2^0 \phi_1^c - p_1^c \phi_2^0)\}$$

$$+ K_i k_y \phi_3^c - \kappa k_3^2 p_3^s, \tag{A18}$$

where $k_1^2 = k_x^2 + k_y^2$, $k_2^2 = 4k_x^2 + k_y^2$, $k_3^2 = 9k_x^2 + k_y^2$, and $k_{xy}^2 = \frac{1}{2}k_x k_y$.

If the third harmonics, $3k_x$, are neglected, the model equtaions above agree with those of the 11 ODE model given by Hu and Horton.[12]

[1] A. M. Dimits, G. Bateman, M. A. Beer *et al.*, Phys. Plasmas **7**, 969 (2000).

[2] G. W. Hammett and F. W. Perkins, Phys. Rev. Lett. **64**, 3019 (1990).

[3] M. A. Beer and G. W. Hammett, Phys. Plasmas **3**, 4046 (1996).

[4] Z. Lin, T. S. Hahm, W. W. Lee, W. M. Tang, and R. B. White, Science **281**, 1835 (1998).

[5] W. Horton, R. D. Estes, and C. Biskamp, Phys. Plasmas **22**, 663 (1980).

[6] S. Hamaguchi and W. Horton, Phys. Fluids B **2**, 1833 (1990).

[7] S. Hamaguchi and W. Horton, Phys. Fluids B **2**, 3040 (1990).

[8] S. Hamaguchi and W. Horton, Phys. Fluids B **4**, 319 (1992).

[9] W. Horton, D-I. Choi, and W. Tang, Phys. Fluids **24**, 1077 (1981).

[10] A. Jarmen, P. Anderson, and J. Weiland, Nucl. Fusion **27**, 941 (1987).

[11] H. Mordman and J. Weiland, Nucl. Fusion **27**, 941 (1987).

[12] G. Hu and W. Horton, Phys. Plasmas **4**, 3262 (1997).

[13] E. N. Lorenz, J. Atoms. Sci. **20**, 130 (1963).

[14] L. N. Howard and R. Krishnamurti, J. Fluid Mech. **170**, 385 (1986).

[15] B. Coppi, J. M. Green, and J. L. Johnson, Nucl. Fusion **6**, 101 (1966).

[16] S. Hamaguchi, Phys. Fluids B **1**, 1416 (1989).

[17] A. Takayama and M. Wakatani, Plasma Phys. Controlled Fusion **38**, 1411 (1996).

[18] A. Takayama, M. Wakatani, and H. Sugama, Phys. Plasmas **3**, 3 (1996).

[19] N. Bian, S. Benkadda, O. E. Garcia, J.-V. Paulsen, and X. Garbet, Phys. Plasmas **10**, 1382 (2003).

[20] K. Takeda, S. Hamaguchi, and M. Wakatani, Plasma Phys. Controlled Fusion **44**, A487 (2002).

[21] Z. Lin, T. S. Hahm, W. W. Lee, W. M. Tang, and P. H. Diamond, Phys. Rev. Lett. **83**, 3645 (1999).

[22] S. V. Bazdenkov and O. P. Pogutse, JETP Lett. **57**, 423 (1993).